Title: **Loss of Tbx3 in mouse eye causes retinal angiogenesis defects reminiscent of human disease**

Derbyshire, M.*[1,2], Akula, S.*[1,2], Wong, A.[1,2], Rawlins, K.[1], Voura, E.[1], Brunken, W.J.[1], Zuber, M.E.[1], Fuhrmann, S.[3], Moon, A.M.[4,5,6], and Viczian A.S[1†].

* these authors contributed equally to this work

† Corresponding author

1, Ophthalmology and Visual Sciences Department, Upstate Medical University, 750 East Adams Street, Syracuse, NY 13210.

2, College of Medicine, Upstate Medical University, 750 East Adams Street, Syracuse, NY 13210.

3, Ophthalmology and Visual Sciences Department, Vanderbilt Eye Institute, Vanderbilt University, Nashville, TE 37232.

4, Department of Molecular and Functional Genomics, Weis Center for Research, Geisinger Clinic, Danville, PA 17822.

5, Department of Human Genetics, University of Utah, Salt Lake City UT 84112

6, The Mindich Child Health and Development Institute, Hess Center for Science and Medicine at Mount Sinai, New York, NY, USA 10029

Word count: 4,193

Funding: This study was supported by the National Institutes of Health (R21 EY029114 to A.S.V; R01 EY012676 to W.J.B; R21 EY030654 to M.E.Z; R01 EY024373 to S.F.), and grants to the Ophthalmology and Visual Sciences Department from Research to Prevent Blindness (Unrestricted Award) and the District 20-Y Lions Club.

Commercial relationship disclosures: none.

Abstract

Purpose: In Retinopathy of Prematurity (ROP), infants often have incomplete vascularization, affecting the temporal region. A factor expressed in this region during retinal development is the T-box factor, *Tbx3*, which has not been studied in the mammalian eye. The purpose of this study was to determine if *Tbx3* is required during eye formation for retinal angiogenesis.

Methods: Conditional removal of *Tbx3* from both retinal progenitors and astrocytes was done using the optic cup-Cre recombinase driver, *BAC-Dkk3-CRE* and analyzed using standard immunohistochemical techniques.

Results: With *Tbx3* loss, the retinas were hypovascular, as seen in patients with ROP and Familial Exudative Vitreoretinopathy (FEVR). Retinal vasculature failed to form the stereotypic tri-layered plexus in the dorsal-temporal region. Astrocyte precursors were reduced in number and failed to form a lattice at the dorsal-temporal edge. We next examined retinal ganglion cells, as they have been shown to play a critical role in retinal angiogenesis. We found that melanopsin expression and Islet1/2-positive retinal ganglion cells were reduced in the dorsal half of the retina. In previous studies, loss of melanopsin has been linked to hyaloid artery persistence, which we also observed in the *Tbx3* cKO retina, as well as in infants with ROP or FEVR.

Conclusions: Together, these results show that TBX3 is required for normal mammalian eye formation for the first time. This potentially provides a new genetic model for retinal hypovascular diseases.

48 **Introduction**

49 Retinal development requires the synchronized formation of neural and vascular tissue
50 for visual function. The early mouse retina remains avascular until differentiation of retinal cells
51 causes an increase in metabolic demand. The differentiated cells release proteins that stimulate
52 the migration and proliferation of astrocytes from the optic nerve just prior to birth[1–3] Astrocyte
53 precursors cling onto the axons of retinal ganglion cells as they migrate into the retina. [4,5]
54 Migrating astrocyte precursors then produce signals to attract endothelial cells into the retina,
55 which in turn, produces proteins that cause the astrocytes to differentiate. Therefore,
56 coordinated activity of neural, astrocytes and endothelial cells are essential for nascent blood
57 vessels to begin forming a steady retinal blood supply. Disruption of signals from either the
58 vascular cells or neurons halts angiogenesis throughout the retina, creating a hypovascular
59 retina seen in Retinopathy of Prematurity (ROP) and Familial Exudative Retinopathy (FEVR). [1]
60 Mutations in Wnt signaling pathway components, like the Wnt receptor Frizzled4, are linked to
61 these syndromes [6–9], and are responsible for 50% of FEVR cases. [1] The genetic mutations
62 causing the remaining half of the FEVR patients are unknown. [1]

63 The signals, which drive creation of the retinal vasculature, function in concert with other
64 signals that cause regression of the vascular source during embryonic development, the hyaloid
65 artery. The hyaloid artery is a transient fetal vascular structure in many vertebrates. Its
66 regression is triggered by signals from intrinsically photosensitive retinal ganglion cells
67 (ipRGCs). [10,11] Failure of the hyaloid vessels to regress leads to persistent fetal vasculature
68 (PFV), which leads to intraocular hemorrhage and impairment of vision. Despite decades of
69 study, and the importance to human disease, a complete understanding the molecular
70 regulation of retinal vascular development is still lacking.

71 In this study, we have identified a key factor, *Tbx3*, in cell types affecting retinal vascular
72 development. In the frog, *Xenopus laevis*, *tbx3* is expressed in the eye field prior to optic vesicle
73 formation where it plays an essential role early in eye formation. [12–16] Later in ocular
74 development, *Tbx3* is found in the dorsal half of the optic cup in both frog and mouse. [13,14,16–18]
75 Functional studies of the role of *Tbx3* in mammalian eye formation have not been done. An
76 initial gene deletion of murine *Tbx3* did not study the eye [19] and produced only a hypomorphic
77 deletion. [20] Thus, a conditional ablation strategy was developed [20,21] and used successfully to
78 study the role of *Tbx3* in several other tissues, including vascular cells during kidney
79 development. [22–28] We investigated the role of *Tbx3* in mammalian retinal development for the
80 first time using a combination of expression studies and reverse genetics to probe function. To
81 our surprise, we found that *Tbx3* is expressed not only in embryonic retinal progenitors, but also
82 in retinal astrocyte precursors at P0. To investigate the effect of *Tbx3* loss-of-function on retinal
83 development, we crossed mice bearing the *Tbx3* conditional allele [20] with a Cre driver, BAC-
84 Dkk3-Cre, that functions in retinal progenitors, astrocytes, but not endothelial cells. [29,30] In the
85 *Tbx3* conditional knockout mice, we observed that the hyaloid artery persisted, and the retina
86 was hypovascular. We found fewer astrocytes in the *Tbx3* conditional knockout retina at P9, and
87 by P30, the astrocytic lattice was malformed in the dorsal retina. With *Tbx3* loss, we also found
88 thinner optic nerves and fewer intrinsically photosensitive retinal ganglion cells. Together, these
89 results suggest that TBX3 is required for mammalian eye formation and that this conditional
90 knockout could potentially be a new mouse model for hypovascular diseases.

91 **Methods**

92 *Mice*

93 Generation of transgenic mouse strains, BAC-Dickkopf3:cre (*BAC-Dkk3-Cre*) [29], *Tie2-Cre*,[31,32]
94 *Tbx3*^{mcm} ,[24] *Tbx3*-floxed and *Tbx3*^{GR},[20,21] were maintained on a C57Bl/6J background. Tamoxifen
95 treatment was done as previously described. [33] Cre activity was assessed using the Ai9 Cre
96 reporter line (B6.Cg-*Gt(ROSA)26Sor*$^{tm9(CAG\text{-}tdTomato)Hze}$/J; The Jackson Laboratory, stock#:
97 007909). We used sibling conditional knockout (*BAC-Dkk3-Cre*$^{+}$;*Tbx3*$^{\Delta Fl/\Delta Fl}$) and wild-type (*BAC-*
98 *Dkk3-Cre*-negative;*Tbx3*$^{Fl/+}$) mice. At least two litters were used for analysis with the number of
99 mice (N) indicated. We observed no difference in levels of TBX3 protein in male and female
100 samples by western blot (Fig. 1L) and thus, performed our analysis on a random mixture of
101 sexes. This study was approved by the Upstate Institutional Animal Care and Use Committee
102 and adheres to the ARVO Statement for the Use of Animals in Ophthalmic and Vision
103 Research.

104 *Genotyping*

105 Ear punches or tail snips (1-2 mm) were incubated overnight at 55˚C in 100 μl lysis buffer
106 (10mM Tris, pH 8.0, 100mM NaCl, 10mM EDTA, pH 8.0, 0.05% SDS) and 80 μg Proteinase K
107 (Sigma; catalog #: P2308; 20 mg/ml stock). Samples were spun down at 14,000g for 15
108 minutes; 70μl supernatant was placed in 200μl ice cold isopropanol; DNA was pelleted at 4˚C,
109 14,000g for 10 minutes and washed twice with 70% ethanol, dried and resuspended in 10 mM
110 Tris, pH 8.0. PCR was performed as described in Table S1 with 0.25 units EconoTaq enzyme
111 (Biosearch Technologies), 1X EconoTaq Buffer, 200μM dNTPs, 0.25μM primers for all
112 reactions, except *Tbx3*^{GR} reactions that included 2% DMSO.

113 *Immunostaining*

114 For sections, isolated eyes were fixed in 4% paraformaldehyde/1X PBS for either 30 min on ice
115 (for *in situ* hybridization or GFP immunostaining) or overnight (for all other immunostaining). The
116 tissue was washed in 1X PBS, and then, incubated with sucrose (5%, 10%, and 20%). The eyes
117 were then mounted in O.C.T. (Tissue-Tek) and sectioned (20μm). We immunostained sections
118 by using conditions that depended on the primary antibody (Table S2). Slides were washed 3
119 times in 1X PBST (1X PBS and 0.1% TritonX) and cover slipped with FluorSave
120 (MilliporeSigma) and 2% DABCO (1,4-Diazabicyclo[2.2.2]octane; Sigma). Flat mounts were
121 stained with isolectin B4 (IB4) and immunostained with antibodies, as described. [34]
122 Reinforcement labels (Avery 5722) were attached to slides, retinas were placed inside each ring
123 with mounting solution [FluorSave (MilliporeSigma) and 2% DABCO, and topped with a round
124 cover slip.

125 *RNA in situ hybridization*

126 RNA was extracted from mouse retinas using RNAzol RT (Molecular Research Center Inc.) and
127 cDNA was generated using GOSCRIPT (Promega) reverse transcriptase according to the
128 manufacture's protocol. *Tbx3* cDNA was PCR amplified with Herculase II (Fisher) using the
129 following primers: BamH1 mTbx3 Forward (5' aatggatccaCCATGAGCCTCTCCATGAG 3') and
130 Xho1 mTbx3 Reverse (5' aattctcgagTTAAGGGGACCCGCTG 3') according to the
131 manufacture's protocol. The PCR product was cut with BamH1 and Xho1 (New England
132 Biolabs) and cloned directly into pCS2R cut with the same enzymes. DIG-labeled sense and
133 antisense cRNA probes were manufactured from linear DNA made using these same two
134 restriction enzymes. In situ hybridization was done as previously described. [35,36]

135 *Microscopy*

136 Images were taken using a Leica DM600B stereomicroscope outfitted with a MicroPublisher 6
137 camera (Teledyne Q-Imaging), and, where applicable, stitched together using the Volocity (v6.3)

138 software. Confocal images were taken with the Zeiss LSM780 confocal and Zeiss Imaging
139 Software. Images of WT and cKO samples were equally processed for brightness and contrast
140 in Adobe Photoshop 2022. Cell counts and analysis were performed under double-blind
141 conditions. Sample types were revealed when entering numbers into the statistics software
142 (Prism v9.3).

143 *Measurement of vasculature*

144 We measured the surface area occupied by retinal structures and the volume using Volocity
145 software. The ratio of retinal structure to whole retinal surface was calculated and statistically
146 analyzed. The migration of Pax2+ cells was measured within 500μm of the dorsal petal
147 (counting 10 cells per sample). The area occupied by Pax2+ cells was measured by adjusting
148 the threshold in ImageJ and comparing that to the area of the dorsal retina.

149 *Western immunoblotting*

150 Protein was extracted from both retinas of sibling newborns and processed for western blot
151 analysis, as previously described [37] Anti-TBX3 antibody (1:2000; Bethyl Lab, Inc.) in 5% milk,
152 0.1% Tween/1XTBS was used.

153 *Statical analysis*

154 Prism (v9.3) was used for statistical analysis. Measurements were done blind to the genotype of
155 the sample. We normalized data by taking the average wild-type measurement in each litter and
156 dividing it into each sample in that litter. To determine the density of OPN4-positive cells, we
157 divided retinal petal surface area (Volocity) into the total cells counted. The average density for
158 WT samples was calculated; this number was used to divide into the density for all sibling
159 samples. Graphs and data are reported as mean ± the standard error of the mean (s.e.m.).
160 Each point on a graph is the average of both eyes from a single animal (N).

161 **Results**

162 To determine the expression pattern of *Tbx3* in the embryonic eye, a tamoxifen-inducible
163 Cre was knocked into the *Tbx3* gene locus (*Tbx3*$^{mcm/+}$) and then crossed with the *Rosa*^{LacZ}
164 reporter line (*Tbx3*$^{mcm/+}$*; Rosa*$^{LacZ/+}$; Fig. 1A, B). [24] Consistent with earlier studies, *LacZ* was
165 expressed at E10.5 and E11.5 in the dorsotemporal region of the optic cup with gradual
166 reduction in the ventral eye. [17,38] *In situ* hybridization to detect *Tbx3* mRNA showed a similar
167 gradient of transcript expression (Fig. 1C,D). In newborn mice, we find that *Tbx3* mRNA is
168 confined to the base of the neuroblast layer (arrows, Fig. 1E-E'') and in cells at the inner limiting
169 membrane (arrowhead, Fig. 1E'). To better visualize TBX3 expression, we used the recombined
170 *Tbx3*^{GFP} conditional reporter allele, *Tbx3*$^{GR/+}$, in which GFP has been knocked into the
171 endogenous *Tbx3* gene (TBX3-GFP). [21] Relatively little GFP staining was detected in wild-type
172 sibling embryos (Fig. 1F), while in *Tbx3*$^{GR/+}$ embryos, we detected embryonic TBX3-GFP in the
173 same gradient pattern with a few GFP-positive cells at the optic nerve head (arrows, Fig. 1G').
174 At E13.5, Pax2 is expressed in the optic nerve head in cells fated toward an astroglial lineage.
175 [3,39,40] We detected GFP at low levels co-staining in some Pax2-positive cells (arrows, Fig. 1G'-
176 G''' and Fig. S1A-B'') with Pearson's correlation co-efficient for GFP/Pax2-positive retinal cells
177 averaged 0.337 ± 0.05 (>4 sections measured per eye; N=2), indicating low correlation. At birth,
178 Pax2 marks astrocyte precursors as they migrate into the retina. [41,42] We flat mounted retinas at
179 P0, immunostained with anti-Pax2 and GFP antibodies, and imaged whole retinas (Fig. S1 C,D
180 and Fig. 1H,I). Flat mounts of P0 retinas from sibling WT have no visible GFP expression, yet
181 TBX3-GFP mice show GFP/Pax2 co-labeling (Fig. 1H,I and Movies 1,2). Together, these data
182 suggest that *Tbx3* is initially expressed in retinal progenitors, and possibly some Pax2-positive
183 glial progenitors while later, it is expressed in astrocyte precursors, as well as cells in the
184 neuroblast layer.
185 To investigate the effects of *Tbx3* loss on early eye formation, we selected the *BAC-*
186 *Dkk3-CRE* mouse line. [29] To confirm its specificity, *BAC-Dkk3-CRE* mice were crossed with the

187 Ai9 reporter line that expresses tdTomato in the presence of CRE activity. As previously
188 reported, we found weak expression of the tdTomato reporter in E9.5 optic vesicles (arrows,
189 Fig. 1J) that was detected throughout the neural retina, optic stalk and in the lens epithelium by
190 E11.5 (Fig. 1K and S1E-E''), but not in endothelial cells (dashed arrow, Fig. S1E''). In *BAC-*
191 *Dkk3-CRE* postnatal retinas, there was a gap in tdTomato expression in blood vessels, but not
192 the surrounding neurons and astrocytes (arrow, Fig. S1F-F'''), confirming that Cre activity was
193 absent in these retinal endothelial cells. To ensure that our protocol detected tdTomato in blood
194 vessels, we used *Tie2-Cre;Ai9* retinal flat mounts stained with the same blood vessel markers,
195 which perfectly matched the expected vascular structures (Fig. S1G-G'''). Together, these
196 results suggest that *BAC-Dkk3-CRE* drives Cre recombinase in neurons, astrocytes, but not
197 endothelial cells. Western blot analysis confirmed the loss of TBX3 protein in the *BAC-Dkk3-*
198 *CRE;Tbx3*$^{\Delta Fl/\Delta Fl}$ retina (Fig. 1L). Preliminary observations indicated abnormal blood vessel
199 formation in the eyes of *BAC-Dkk3-CRE;Tbx3*$^{\Delta Fl/\Delta Fl}$ mice. Therefore, we investigated the effect of
200 *Tbx3* loss on retinal vasculature development.

201 Retinal vasculature develops postnatally in mice and blood vessels reach the edge of
202 the retina by P9. [43,44] Therefore, to determine the effect of *Tbx3* loss on angiogenesis, we
203 stained P9 retinal flat mounts using isolectin B4 (IB4) to visualize vascular endothelial cells (Fig.
204 2A,A'). *BAC-Dkk3-CRE;Tbx3*$^{\Delta Fl/\Delta Fl}$ mice (*Tbx3* cKO) had severe disruption of vasculature
205 development, in that the blood vessels failed to advance to the edges of the retina (Fig. 2B,B').
206 The hyaloid artery (HA) regresses postnatally and is substantially reduced by P8. [11] While we
207 observed remnants of this structure in some wild-type samples (arrow, Fig. 2A'), the vessel
208 were easily observed in *Tbx3* cKO retinas (Fig. 2B,B'). Measuring retinal surface areas covered
209 by the vasculature (Fig. 2C), we found a decrease in the ventral vascular coverage in comparing
210 *Tbx3* cKO and wild-type siblings (71 ± 5.9%), yet the dorsal *Tbx3* cKO retina exhibited more
211 loss (Fig.2C; 24.9 ± 3.0%). These results indicate a requirement for *Tbx3* in the normal

212 development or maintenance of the early postnatal retina vasculature. It is also possible that
213 *Tbx3* loss simply causes a delay in forming the retinal vasculature, so we next looked at blood
214 vessels after they matured.

215 Retinas were collected from P26 mice to determine the effect of *Tbx3* loss on the mature
216 vascular plexus. In contrast to the wild-type structure (Fig. 3A-C), the vascular plexus of *Tbx3*
217 cKO retinas was abnormal (Fig. 3D-F). Confocal optical sections showed the superficial layer
218 did not extend to the dorsotemporal peripheral retina in *Tbx3* cKO mice (Fig. 3D,F, dashed red
219 line marks areas; Movie 3). In addition, the dorsal vein was thinner and missing from the edge of
220 conditional knockout retinas (red arrowheads, Fig. 3G vs. 3H; Movie 3). The *Tbx3* cKO vascular
221 plexus also appeared less complex when compared to wild-type siblings (Fig. 3G,H). To further
222 define the apparent reduction in complexity, we measured both the vasculature's branch point
223 and length density in *Tbx3* cKO and wild-type animals (Fig. 3I; quantitation shown in Fig. S2).
224 We found a reduction in both branch point density (WT, 1537 ± 99; cKO, 1034 ± 106
225 junctions/mm^2) and vascular length density (WT, 6.48 ± 0.12; cKO, 5.20 ± 0.26 mm/mm^2) in
226 mutants (Fig. 3I). Confocal imaging of central retinal sections from controls showed the normal
227 tri-layered vasculature and inter-plexus branching (Fig. 3J and Movie 4). In contrast, *Tbx3* cKO
228 retinas lacked the superficial plexus (Fig. 3K and Movie 5). Cryostat sections show vessels in all
229 three layers in the wild-type (Fig. 3L and Fig. S3A), while in the absence of *Tbx3*, some regions
230 (as in dashed regions shown in Fig. 3F) were missing both the superficial and deep layers (Fig.
231 3M and Fig. S3B). Glial fibrillary acidic protein (GFAP) labels Müller glia and astrocytes at this
232 age. We detected less dense GFAP staining in the *Tbx3* cKO retina and that the outer nuclear
233 layer is thinner at the dorsal edge in the mutants (bracket, Fig. 3M). Less GFAP staining
234 suggests fewer astrocytes in the *Tbx3* cKO retina. Together, these results indicate that the
235 formation of a normal adult retinal vasculature requires *Tbx3*.

236 If the reduction in angiogenesis in the *Tbx3* cKO begins at this early time point, then we
237 would expect the lattice to be disrupted in mutant mice. Flat mounts at P2 showed reduced
238 endothelial cells and astrocytes in the *Tbx3* cKO retina (Fig. 4B,B'). Retinal astrocyte precursors
239 express the paired-box transcription factor, Pax2, and the growth factor receptor, PDGFRα, and,
240 as they mature express not glial fibrillary acidic protein (GFAP). [41,42] We found stunted migration
241 and fewer Pax2-positive astrocyte precursors in the dorsal and ventral retinas at P2 (Fig. 4C-F).
242 As we found TBX3 expressed in early astrocyte precursors (Fig. 1I), the stunted growth or
243 migration of astrocyte precursors suggests that TBX3 may be required by these cells as they
244 move into the retina. We further reasoned that lattice formation may recover if TBX3 is only
245 required at this initial stage, and therefore, next looked at older animals.
246 By P9, astrocytes reached the edge of the wild-type retina (Fig. 5A), yet failed to do so in
247 the conditional knockout (Fig. 5B). Even at one month of age, astrocytes failed to reach the
248 dorsal edge of the cKO retinas (compare Fig. 5C to 5D,D'). Double labeling astrocytes and
249 endothelial cells, we found an abnormal vascular plexus in areas without a stereotypical
250 astrocyte lattice (Fig. 5D'-D'''). We compared the surface area occupied by astrocytes at P9 and
251 P30, normalized to the average wild-type retinal surface area. We observed a statistically
252 significant difference between wild-type and *Tbx3* cKO retinas at P9 and P30 (P9 WT, 1.0 ±
253 0.01; P9 cKO, 0.58 ±0.02; P30 WT, 0.97±0.01; P30 cKO, 0.76 ±0.03; Fig. 5E). We also
254 observed significant growth between P9 and P30 ($p<0.001$), indicating that signals promoting
255 astrocyte lattice formation persist in the absence of TBX3 (Fig. 5E). These results indicate that
256 astrocytes require TBX3 to form the astrocytic lattice required for normal retinal vasculature
257 formation. Astrocyte lattice formation can also be disrupted with the loss of retinal ganglion cells,
258 as in the *Atoh7* knockout retina. These mice grow a severely stunted astrocytic lattice. [4,45] Thus,
259 it is possible that TBX3 is indirectly affecting astrocytes by functioning within ganglion cells.
260 Previous studies have also shown that hyaloid artery regression is dependent on signals from

261 intrinsically photosensitive retinal ganglion cells. [10,11] We observed that the hyaloid artery
262 persisted in the mutant retina (Figs. 2B,B' and 5B). Therefore, we next investigated whether
263 retinal ganglion cell formation requires TBX3.

264 We found that optic nerves were significantly thinner in cKO mice compared to their WT
265 littermates (Fig. 6A-C), measuring 71 ± 3.9% of the average WT optic nerve (Fig. 6D). Using the
266 anti-Islet1/2 antibody, we observed a significant decrease in dorsal Islet1/2-positive retinal
267 ganglion cells (RGCs) in the cKO retina, but no difference in the ventral region (dorsal WT: 37.7
268 ± 2.8 cells; dorsal cKO: 27.7 ± 2.4 cells; Fig. 6E-G). This suggests that *Tbx3* is required by a
269 subset of Islet1/2-expressing dorsal RGCs. Islet1 is thought to regulate the formation of most
270 RGCs, including melanopsin-expressing (OPN4) intrinsically-photosensitive ganglion cells
271 (ipRGCs). [46] We stained flat mounts with the anti-OPN4 antibody and measured the density of
272 OPN4-positive cells for each sample, normalized to the average wild-type control. When blood
273 vessels were stunted at P9, we observed significant reduction of ipRGC density in the dorsal
274 (WT: 1.00 ± 0.11; cKO: 0.57 ± 0.06) and nasal/temporal petals (WT: 0.83 ± 0.07; cKO: 0.46 ±
275 0.06), but not in the ventral petals (Fig. 6H-J). Overall, we found significantly less ipRGCs in
276 cKO retinas at P9 (WT: 1.00 ± 0.10; cKO: 0.63 ± 0.09). This difference persists when measured
277 at P30 (WT: 1.00 ± 0.09; cKO: 0.68 ± 0.02), suggesting that the reduction in ipRGCs was not
278 due to a delay of differentiation (Fig. 6K-L). Together, these results indicate that TBX3 is
279 required for a subset of OPN4-expressing ipRGCs in the dorsal half of the retina, which control
280 vascular formation in this region.

281

282 **Discussion**

283 Our results provide the first evidence that TBX3 is required for mammalian eye
284 formation. We have found that *Tbx3* mRNA and protein is expressed in embryonic retinal

285 progenitors and postnatal astrocyte precursor cells. When we remove *Tbx3* from the embryonic
286 optic cup, the hyaloid artery persists in P9 mice and retinal vascular formation is stunted. At P9,
287 the vascular defect is found throughout the retina, but more severe in the dorsal region. The
288 dorsal vascular plexus continues to be affected by *Tbx3* loss in the older animals, including the
289 loss of the superficial layer of the vascular plexus and the astrocyte lattice. We observe that in
290 the absence of *Tbx3,* fewer astrocyte precursors are present in the retina. As the retina
291 matures, astrocyte lattice formation recovers in all but the dorsal region. To our knowledge,
292 localization of the defect to the dorsal intraretinal vasculature is the first report of a spatially
293 distinct defect in this vascular bed. In contrast, loss of Aldh1a1, also expressed in dorsal retinal
294 neurons affects the dorsal choroidal, or outer retinal vasculature. [47] In the dorsal neural retina
295 area with *Tbx3* conditionally removed, we find fewer Islet1/2-positive and melanopsin-
296 expressing intrinsically photosensitive retinal ganglion cells. One interpretation is that these
297 neurons fail to attract or stimulate the proliferation and/or migration of astrocyte precursors that
298 form the dorsal lattice. In contrast, our data could also suggest that TBX3 may function within
299 astrocytes, controlling their development and loss of *Tbx3* in retinal progenitor cells, which
300 affects dorsal retinal ganglion cells, simply causes hyaloid artery persistence at P9 in the *Tbx3*
301 cKO retina. The fact that we are observing abnormal vascular plexus and astrocyte formation in
302 the dorsal retina, supports the hypothesis that the underlying defect is the loss of dorsal retinal
303 ganglion cells. In any case, these mice provide a fruitful new model to study retinal
304 hypovascularization.

305 Patients with syndromes, including Norrie disease (ND) or Familial Exudative
306 Vitreoretinopathy (FEVR), develop hypovascular retinas that lead to congenital blindness. [48]
307 These diseases have been associated with mutations in Wnt/Norrie signaling pathway ligands
308 (*LRP5*, *NDP*), receptor (FZ4) and a co-receptor (*TSPAN12*), as well as a kinesin family member
309 11 (*KIF11*). [6–9] Mutations found in these proteins have been studied using mouse models of

310 these mutant alleles. [48–53] Canonical Wnt signaling occurs when Wnt ligands bind to their
311 receptors, which leads to stabilizing β-catenin that can regulate target downstream genes. While
312 most of these factors work in the canonical Wnt/Norrie signaling pathway, *KIF11* has been
313 shown to function independently from β-catenin signaling in retinal angiogenesis. [48] In separate
314 studies, TBX3 has been shown to work in Wnt signaling and with a kinesin protein. In pull-down
315 assays, TBX3 has direct interaction with another kinesin family member, KIF7, and affects its
316 function. [24] In vivo, TBX3 has been shown to work with, or downstream of, the Wnt signaling
317 pathway in ureter, lung and human colorectal cancer. [23,26,54] In future studies, we plan to
318 determine in which molecular pathway Tbx3 functions.

319 Another characteristic, besides hypovascularization, shared among some FEVR patients
320 is a persistent hyaloid artery. [55–59] In mice, this defect has also been found with the loss of
321 melanopsin (*OPN4*), however, in these mutant mice, the retina is hypervascular, rather than
322 hypovascular. [11] In contrast, the *Tbx3* cKO has a persistent hyaloid artery as well as a
323 hypovascular retina. Along with FEVR, these phenotypes are also present in a mouse model of
324 Retinopathy of Prematurity, in which neonatal pups are exposed to elevated oxygen levels from
325 P0 to P4. [60] In these mice, angiogenesis is globally affected, where only about 25% of the entire
326 retinal surface was covered by P8. [60] In comparison, vessels covered approximately 25% of the
327 dorsal *Tbx3* cKO retina. Therefore, it is possible that Tbx3 is required for the hypoxia signaling
328 pathway either in neurons or in astrocytes. Moreover, the similarities between the phenotypic
329 changes we observe in the conditional *Tbx3* knockout mouse and those in FEVR/ROP patients
330 suggests the exciting possibility that the *Tbx3* cKO may serve as a new mouse model for these
331 human diseases.

332 We discovered that TBX3-GFP is expressed in astrocyte precursors. We found that
333 *Tbx3* loss causes a reduction in astrocyte precursors in the newborn retina. Astrocytes arise
334 from the optic disc progenitor zone which surrounds the optic nerve disc. [42,61] During migration

335 into the retina, they proliferate prior to contact with endothelial cells, since the endothelial cells
336 cause their differentiation. [61] Our results could be explained by either a reduction in astrocyte
337 precursor proliferation or reduced migration due to corrupt cues from the neural retina lacking
338 *Tbx3*. Retinal ganglion cells release platelet-derived growth factor A-chain (PDGF-A), which
339 attracts astrocytes, but PDGF-A also causes proliferation of these cells. [62] As we have also
340 observed a loss of RGCs in the dorsal retina, it is possible that loss of *Tbx3* indirectly affects
341 astrocyte proliferation/migration. It is also possible that in astrocyte precursors TBX3 contributes
342 to the regulation of a gene that controls astrocyte proliferation - like the transcription factor
343 Tailless (*Tlx*). [63,64] We previously found that misexpression of frog *tbx3* (also known as ET for
344 'Eye T-box') induced *tll* expression. [15] It will be important to investigate the role of TBX3 in
345 regulating *Tlx* expression and astrocyte proliferation and/or migration.
346 Later, in the differentiated retina we found truncation of the astrocytic lattice in the
347 dorsal-temporal region. Blood vessels were growing into the area, but they failed to form a
348 superficial plexus. Endothelial cells build the superficial plexus in response to the chemical and
349 structural cues of the underlying astrocytes. [65–69] Therefore, it is logical that loss of dorsal
350 astrocytes due to loss of *Tbx3* would lead to superficial plexus loss in that region. Finding dorsal
351 intermediate blood vessels in the absence of the superficial and sometimes deep layers is
352 curious. The deep plexus formation has been linked to spontaneous activity from cholinergic
353 starburst amacrine cells. [70] Meanwhile, formation of the superficial and deep, but not
354 intermediate, plexus layers requires the activity of the hypoxic response pathway (via the von
355 Hippel-Lindau factor (Vhl) found in amacrine and horizontal cells. [71] In a recent study that used
356 single cell PCR to generate a genetic regulatory network in the mouse retina, *Tbx3* was found in
357 amacrine and Müller glia. [72] Overexpression of TBX3 in retinal progenitors at P0 led to an
358 increase of amacrine, retinal ganglion cells, Müller glia, and bipolar cells, but repressed

359 formation of rod photoreceptors. [72] Therefore, in future studies, we will determine the effect of
360 *Tbx3* loss on all types of retinal neurons.

361 **Acknowledgments**

362 We would like to thank Jason Shandler, Robertha Barnes, Amanda Bielecki, Abigail Snow,
363 Stephen Sanabria and Dominica Colavito for their excellent technical assistance. We would also
364 like to thank Dr. Arvydas Matiukas for his assistance in using the confocal microscope in
365 Neuroscience Microscopy Core. The anti-Islet1/2 antibody was obtained from the
366 Developmental Studies Hybridoma Bank, created by the NICHD of the NIH and maintained at
367 The University of Iowa, Department of Biology, Iowa City, IA 52242.

368 **References**

369 1. Selvam, S., Kumar, T. & Fruttiger, M. Retinal vasculature development in health and
370 disease. *Prog Retin Eye Res* 2018;63:1-19.
371 2. Sun, Y. & Smith, L. E. H. Retinal Vasculature in Development and Diseases. *Annu Rev Vis*
372 *Sci* 2018;4:101-122.
373 3. Tao, C. & Zhang, X. Development of astrocytes in the vertebrate eye. *Dev Dyn*
374 2014;243:1501-1510.
375 4. O'Sullivan, M. L., Puñal, V. M., Kerstein, P. C. et al. Astrocytes follow ganglion cell axons
376 to establish an angiogenic template during retinal development. *Glia* 2017;65:1697-1716.
377 5. Paisley, C. E. & Kay, J. N. Seeing stars: Development and function of retinal astrocytes.
378 *Dev Biol* 2021;478:144-154.
379 6. Li, J. K., Li, Y., Zhang, X. et al. Spectrum of Variants in 389 Chinese Probands With
380 Familial Exudative Vitreoretinopathy. *Invest Ophthalmol Vis Sci* 2018;59:5368-5381.
381 7. Rao, F. Q., Cai, X. B., Cheng, F. F. et al. Mutations in LRP5,FZD4, TSPAN12, NDP,
382 ZNF408, or KIF11 Genes Account for 38.7% of Chinese Patients With Familial Exudative
383 Vitreoretinopathy. *Invest Ophthalmol Vis Sci* 2017;58:2623-2629.

384 8. Tang, M., Sun, L., Hu, A. et al. Mutation Spectrum of the LRP5, NDP, and TSPAN12
385 Genes in Chinese Patients With Familial Exudative Vitreoretinopathy. *Invest Ophthalmol*
386 *Vis Sci* 2017;58:5949-5957.
387 9. Tauqeer, Z. & Yonekawa, Y. Familial Exudative Vitreoretinopathy: Pathophysiology,
388 Diagnosis, and Management. *Asia Pac J Ophthalmol (Phila)* 2018;7:176-182.
389 10. Nguyen, M. T., Vemaraju, S., Nayak, G. et al. An opsin 5-dopamine pathway mediates
390 light-dependent vascular development in the eye. *Nat Cell Biol* 2019;21:420-429.
391 11. Rao, S., Chun, C., Fan, J. et al. A direct and melanopsin-dependent fetal light response
392 regulates mouse eye development. *Nature* 2013
393 12. Motahari, Z., Martinez-De Luna, R. I., Viczian, A. S. & Zuber, M. E. Tbx3 represses bmp4
394 expression and with Pax6 is required and sufficient for retina formation. *Development*
395 2016;143:3560-3572.
396 13. Weidgang, C. E., Russell, R., Tata, P. R. et al. TBX3 Directs Cell-Fate Decision toward
397 Mesendoderm. *Stem Cell Reports* 2013;1:248-265.
398 14. Wong, K., Peng, Y., Kung, H. F. & He, M. L. Retina dorsal/ventral patterning by Xenopus
399 TBX3. *Biochem Biophys Res Commun* 2002;290:737-742.
400 15. Zuber, M. E., Gestri, G., Viczian, A. S., Barsacchi, G. & Harris, W. A. Specification of the
401 vertebrate eye by a network of eye field transcription factors. *Development*
402 2003;130:5155-5167.
403 16. Takabatake, Y., Takabatake, T. & Takeshima, K. Conserved and divergent expression of
404 T-box genes Tbx2-Tbx5 in Xenopus. *Mech Dev* 2000;91:433-437.
405 17. Chapman, D. L., Garvey, N., Hancock, S. et al. Expression of the T-box family genes,
406 Tbx1-Tbx5, during early mouse development. *Dev Dyn* 1996;206:379-390.

407 18. Sowden, J. C., Holt, J. K., Meins, M., Smith, H. K. & Bhattacharya, S. S. Expression of
408 Drosophila omb-related T-box genes in the developing human and mouse neural retina.
409 *Invest Ophthalmol Vis Sci* 2001;42:3095-3102.
410 19. Davenport, T. G., Jerome-Majewska, L. A. & Papaioannou, V. E. Mammary gland, limb
411 and yolk sac defects in mice lacking Tbx3, the gene mutated in human ulnar mammary
412 syndrome. *Development* 2003;130:2263-2273.
413 20. Frank, D. U., Emechebe, U., Thomas, K. R. & Moon, A. M. Mouse TBX3 mutants suggest
414 novel molecular mechanisms for Ulnar-mammary syndrome. *PLoS One* 2013;8:e67841.
415 21. Frank, D. U., Carter, K. L., Thomas, K. R. et al. Lethal arrhythmias in Tbx3-deficient mice
416 reveal extreme dosage sensitivity of cardiac conduction system function and homeostasis.
417 *Proc Natl Acad Sci U S A* 2012;109:154-163.
418 22. Barry, D. M., McMillan, E. A., Kunar, B. et al. Molecular determinants of nephron vascular
419 specialization in the kidney. *Nat Commun* 2019;10:5705.
420 23. Aydoğdu, N., Rudat, C., Trowe, M. O. et al. TBX2 and TBX3 act downstream of canonical
421 WNT signaling in patterning and differentiation of the mouse ureteric mesenchyme.
422 *Development* 2018;145
423 24. Emechebe, U., Kumar P, P., Rozenberg, J. M. et al. T-box3 is a ciliary protein and
424 regulates stability of the Gli3 transcription factor to control digit number. *Elife* 2016;5
425 25. Kumar P, P., Franklin, S., Emechebe, U. et al. TBX3 regulates splicing in vivo: a novel
426 molecular mechanism for Ulnar-mammary syndrome. *PLoS Genet* 2014;10:e1004247.
427 26. Lüdtke, T. H., Rudat, C., Wojahn, I. et al. Tbx2 and Tbx3 Act Downstream of Shh to
428 Maintain Canonical Wnt Signaling during Branching Morphogenesis of the Murine Lung.
429 *Dev Cell* 2016;39:239-253.
430 27. Quarta, C., Fisette, A., Xu, Y. et al. Functional identity of hypothalamic melanocortin
431 neurons depends on Tbx3. *Nature Metabolism* 2019;1:222.

432 28. Kaiser, M., Wojahn, I., Rudat, C. et al. Regulation of otocyst patterning by Tbx2 and Tbx3
433 is required for inner ear morphogenesis in the mouse. *Development* 2021dev.195651.
434 29. Sato, S., Inoue, T., Terada, K. et al. Dkk3-Cre BAC transgenic mouse line: a tool for highly
435 efficient gene deletion in retinal progenitor cells. *Genesis* 2007;45:502-507.
436 30. Vigouroux, R. J., Cesar, Q., Chédotal, A. & Nguyen-Ba-Charvet, K. T. Revisiting the role of
437 Dcc in visual system development with a novel eye clearing method. *Elife* 2020;9
438 31. Biswas, S., Watters, J., Bachay, G. et al. Laminin-dystroglycan signaling regulates retinal
439 arteriogenesis. *FASEB J* 2018fj201800232R.
440 32. Kisanuki, Y. Y., Hammer, R. E., Miyazaki, J., Williams, S. C., Richardson, J. A. &
441 Yanagisawa, M. Tie2-Cre transgenic mice: a new model for endothelial cell-lineage
442 analysis in vivo. *Dev Biol* 2001;230:230-242.
443 33. Park, E. J., Sun, X., Nichol, P., Saijoh, Y., Martin, J. F. & Moon, A. M. System for
444 tamoxifen-inducible expression of cre-recombinase from the Foxa2 locus in mice. *Dev Dyn*
445 2008;237:447-453.
446 34. Gnanaguru, G., Bachay, G., Biswas, S., Pinzon-Duarte, G., Hunter, D. D. & Brunken, W. J.
447 Laminins containing the beta2 and gamma3 chains regulate astrocyte migration and
448 angiogenesis in the retina. *Development* 2013;140:2050-2060.
449 35. Viczian, A. S., Vignali, R., Zuber, M. E., Barsacchi, G. & Harris, W. A. XOtx5b and XOtx2
450 regulate photoreceptor and bipolar fates in the Xenopus retina. *Development*
451 2003;130:1281-1294.
452 36. Martinez-De Luna, R. I., Ku, R. Y., Lyou, Y. & Zuber, M. E. Maturin is a novel protein
453 required for differentiation during primary neurogenesis. *Dev Biol* 2013;384:26-40.
454 37. Wong, K. A., Trembley, M., Abd Wahab, S. & Viczian, A. S. Efficient retina formation
455 requires suppression of both Activin and BMP signaling pathways in pluripotent cells. *Biol*
456 *Open* 2015;4:573-583.

457 38. Behesti, H., Holt, J. K. & Sowden, J. C. The level of BMP4 signaling is critical for the
458 regulation of distinct T-box gene expression domains and growth along the dorso-ventral
459 axis of the optic cup. *BMC Dev Biol* 2006;6:62.
460 39. Bosze, B., Suarez-Navarro, J., Soofi, A., Lauderdale, J. D., Dressler, G. R. & Brown, N. L.
461 Multiple roles for Pax2 in the embryonic mouse eye. *Dev Biol* 2021
462 40. Soukkarieh, C., Agius, E., Soula, C. & Cochard, P. Pax2 regulates neuronal-glial cell fate
463 choice in the embryonic optic nerve. *Dev Biol* 2007;303:800-813.
464 41. Chu, Y., Hughes, S. & Chan-Ling, T. Differentiation and migration of astrocyte precursor
465 cells and astrocytes in human fetal retina: relevance to optic nerve coloboma. *FASEB J*
466 2001;15:2013-2015.
467 42. Mi, H. & Barres, B. A. Purification and characterization of astrocyte precursor cells in the
468 developing rat optic nerve. *J Neurosci* 1999;19:1049-1061.
469 43. Stalmans, I., Ng, Y. S., Rohan, R. et al. Arteriolar and venular patterning in retinas of mice
470 selectively expressing VEGF isoforms. *J Clin Invest* 2002;109:327-336.
471 44. Dorrell, M. I., Aguilar, E. & Friedlander, M. Retinal vascular development is mediated by
472 endothelial filopodia, a preexisting astrocytic template and specific R-cadherin adhesion.
473 *Invest Ophthalmol Vis Sci* 2002;43:3500-3510.
474 45. Edwards, M. M., McLeod, D. S., Li, R. et al. The deletion of Math5 disrupts retinal blood
475 vessel and glial development in mice. *Exp Eye Res* 2012;96:147-156.
476 46. Mao, C. A., Li, H., Zhang, Z. et al. T-box transcription regulator Tbr2 is essential for the
477 formation and maintenance of Opn4/melanopsin-expressing intrinsically photosensitive
478 retinal ganglion cells. *J Neurosci* 2014;34:13083-13095.
479 47. Goto, S., Onishi, A., Misaki, K. et al. Neural retina-specific Aldh1a1 controls dorsal
480 choroidal vascular development via Sox9 expression in retinal pigment epithelial cells.
481 *Elife* 2018;7:e32358.

482 48. Wang, Y., Smallwood, P. M., Williams, J. & Nathans, J. A mouse model for Kinesin Family
483 Member 11 (Kif11)-associated familial exudative vitreoretinopathy. *Hum Mol Genet* 2020
484 49. Luhmann, U. F., Lin, J., Acar, N. et al. Role of the Norrie disease pseudoglioma gene in
485 sprouting angiogenesis during development of the retinal vasculature. *Invest Ophthalmol*
486 *Vis Sci* 2005;46:3372-3382.
487 50. Ye, X., Wang, Y., Cahill, H. et al. Norrin, frizzled-4, and Lrp5 signaling in endothelial cells
488 controls a genetic program for retinal vascularization. *Cell* 2009;139:285-298.
489 51. Junge, H. J., Yang, S., Burton, J. B. et al. TSPAN12 regulates retinal vascular
490 development by promoting Norrin- but not Wnt-induced FZD4/beta-catenin signaling. *Cell*
491 2009;139:299-311.
492 52. Ye, X., Wang, Y. & Nathans, J. The Norrin/Frizzled4 signaling pathway in retinal vascular
493 development and disease. *Trends Mol Med* 2010;16:417-425.
494 53. Collin, R. W., Nikopoulos, K., Dona, M. et al. ZNF408 is mutated in familial exudative
495 vitreoretinopathy and is crucial for the development of zebrafish retinal vasculature. *Proc*
496 *Natl Acad Sci U S A* 2013;110:9856-9861.
497 54. Zimmerli, D., Borrelli, C., Jauregi-Miguel, A. et al. TBX3 acts as tissue-specific component
498 of the Wnt/β-catenin transcriptional complex. *Elife* 2020;9
499 55. Dhingra, S., Shears, D. J., Blake, V., Stewart, H. & Patel, C. K. Advanced bilateral
500 persistent fetal vasculature associated with a novel mutation in the Norrie gene. *Br J*
501 *Ophthalmol* 2006;90:1324-1325.
502 56. Payabvash, S., Anderson, J. S. & Nascene, D. R. Bilateral persistent fetal vasculature due
503 to a mutation in the Norrie disease protein gene. *Neuroradiol J* 2015;28:623-627.
504 57. Pendergast, S. D., Trese, M. T., Liu, X. & Shastry, B. S. Study of the Norrie disease gene
505 in 2 patients with bilateral persistent hyperplastic primary vitreous. *Arch Ophthalmol*
506 1998;116:381-382.

507 58. Robitaille, J. M., Wallace, K., Zheng, B. et al. Phenotypic overlap of familial exudative
508 vitreoretinopathy (FEVR) with persistent fetal vasculature (PFV) caused by FZD4
509 mutations in two distinct pedigrees. *Ophthalmic Genet* 2009;30:23-30.
510 59. Wu, W. C., Drenser, K., Trese, M., Capone, A. & Dailey, W. Retinal phenotype-genotype
511 correlation of pediatric patients expressing mutations in the Norrie disease gene. *Arch*
512 *Ophthalmol* 2007;125:225-230.
513 60. Perelli, R. M., O'Sullivan, M. L., Zarnick, S. & Kay, J. N. Environmental oxygen regulates
514 astrocyte proliferation to guide angiogenesis during retinal development. *Development*
515 2021;148:dev199418.
516 61. Mi, H., Haeberle, H. & Barres, B. A. Induction of astrocyte differentiation by endothelial
517 cells. *J Neurosci* 2001;21:1538-1547.
518 62. Fruttiger, M., Calver, A. R., Krüger, W. H. et al. PDGF mediates a neuron-astrocyte
519 interaction in the developing retina. *Neuron* 1996;17:1117-1131.
520 63. Miyawaki, T., Uemura, A., Dezawa, M. et al. Tlx, an orphan nuclear receptor, regulates cell
521 numbers and astrocyte development in the developing retina. *J Neurosci* 2004;24:8124-
522 8134.
523 64. Uemura, A., Kusuhara, S., Wiegand, S. J., Yu, R. T. & Nishikawa, S. Tlx acts as a
524 proangiogenic switch by regulating extracellular assembly of fibronectin matrices in retinal
525 astrocytes. *J Clin Invest* 2006;116:369-377.
526 65. Jiang, B., Liou, G. I., Behzadian, M. A. & Caldwell, R. B. Astrocytes modulate retinal
527 vasculogenesis: effects on fibronectin expression. *J Cell Sci* 1994;107:2499-2508.
528 66. Jiang, B., Bezhadian, M. A. & Caldwell, R. B. Astrocytes modulate retinal vasculogenesis:
529 effects on endothelial cell differentiation. *Glia* 1995;15:1-10.
530 67. Fruttiger, M. Development of the retinal vasculature. *Angiogenesis* 2007;10:77-88.

531 68. Stone, J., Itin, A., Alon, T. et al. Development of retinal vasculature is mediated by
532 hypoxia-induced vascular endothelial growth factor (VEGF) expression by neuroglia. *J*
533 *Neurosci* 1995;15:4738-4747.
534 69. Zhang, Y. & Stone, J. Role of astrocytes in the control of developing retinal vessels. *Invest*
535 *Ophthalmol Vis Sci* 1997;38:1653-1666.
536 70. Weiner, G. A., Shah, S. H., Angelopoulos, C. M. et al. Cholinergic neural activity directs
537 retinal layer-specific angiogenesis and blood retinal barrier formation. *Nat Commun*
538 2019;10:2477.
539 71. Usui, Y., Westenskow, P. D., Kurihara, T. et al. Neurovascular crosstalk between
540 interneurons and capillaries is required for vision. *J Clin Invest* 2015;125:2335-2346.
541 72. Lyu, P., Hoang, T., Santiago, C. P. et al. Gene regulatory networks controlling temporal
542 patterning, neurogenesis, and cell-fate specification in mammalian retina. *Cell Rep*
543 2021;37:109994.
544

545 **Figure Legends**

546 **Figure 1. TBX3 expression in the neural retina and efficient conditional knock-out (cKO)**
547 **using the *BAC-DKK3-Cre* driver.**

548 A,B) LacZ activity under the control of the endogenous *Tbx3*-locus (LacZ KI: *Tbx3*^{mcm}). Arrow
549 points to the dorsotemporal region of the eye at embryonic days 10.5 (E10.5) and 11.5 (E11.5).
550 (C-D') *In situ* hybridization using *Tbx3* antisense RNA at E10.5 and E11.5. Outline of developing
551 eye in C,D; pRPE, presumptive RPE; NR, neural retina. (E) *Tbx3* mRNA expression in newborn
552 retina. (E',E") Inlays of dorsal and ventral retinas. Arrows point to cells at the base of the
553 neuroblast layer (NBL) and arrowhead to cells at inner limiting membrane adjacent to the
554 ganglion cell layer (GCL). (F) Wild-type sibling of transgenic embryo (G) expressing GFP under
555 the control of the endogenous *Tbx3*-locus (*Tbx3*$^{GR/+}$) immunostained with anti-GFP antibody
556 (green) at E13.5. Dashed box shows region magnified. (G'-G''') Close-up of boxed region in G
557 immunostained with an anti-Pax2 (red) and GFP antibodies (see Fig. S1 for more images). (H)
558 Confocal flat mount image of newborn retina from sibling wild-type and (I) *Tbx3*$^{GR/+}$ mice
559 immunostained with anti-Pax2 and GFP antibodies. Orthogonal view on top and side. Arrow
560 points to cell that is positive for Pax2 in H and positive to Pax2 and GFP in I. (J,K) *BAC-Dkk3-*
561 *CRE* expression pattern is detected using Ai9 reporter line expressing tdTomato. Cre activity is
562 first detectable in the optic vessicle (dashed lines) at E9.5 (arrows) and is expressed throughout
563 the neural retina (NR), lens epithelium (LE) and optic stalk (OS) by E11.5. (L) Western blot of
564 P0 retinas collected from wild-type (WT, *Tbx3*$^{Fl/+}$), heterozygous (Het, *BAC-Dkk3-*
565 *CRE;Tbx3*$^{\Delta Fl/+}$), and homozygous knockout (cKO, *BAC-Dkk3-CRE;Tbx3*$^{\Delta Fl/\Delta Fl}$) siblings. Graph
566 shows mean ± s.e.m. of 2 litters. No statistical differences in *Tbx3* expression were observed in
567 males and females. Ordinary one-way ANOVA test with multiple comparisons was used to
568 determine statistical significance. ****, p=0.00005; **, p≤0.01.

569 **Figure 2. Tbx3 loss results in abnormal blood vessel development.**

570 (A,A') Flat mount P9 retinas from wild-type (WT) and (B,B') conditional *Tbx3* knockout retinas
571 (cKO) stained with isolectin GS-B4 (IB4, green) in left and right eyes. Arrows indicate location of
572 hyaloid artery (HA). C) Ratio of the vascularized to total retinal surface area in the dorsal and
573 ventral retina normalized to average WT in each litter. A 2way ANOVA with Šidák's multiple
574 comparisons test was used; ****, $p \leq 0.0001$; *, $p=0.01$.

575 **Figure 3. *Tbx3* cKO retina fails to form superficial plexus in the adult dorsal retina.**

576 (A-F) Confocal flat mount images of P26 dorsal retinas from wild-type (WT; A,B,C) and
577 conditional knockout (cKO; D,E,F) mice stained with isolectin GS-B4 (IB4). Confocal images are
578 inverted. The superficial (A,D), intermediate (B,E) and deep (C,F) plexus from the same retinal
579 flat mounts are shown. (G,H) Maximal projection images from a stereomicroscope
580 simultaneously showing all three plexi from the region indicated in B and E. Artery (black
581 arrows) and vein (red arrowheads) in each panel are marked. (I) Branching index (branch
582 points/retinal surface area) and vascular length density (vessel length/retinal surface area) from
583 maximum projections images (see Fig. S2 for quantitation). Statistical significance was
584 determined using an unpaired, two-tailed T-test; p-values on graph. (J,K) Still 3D rendered
585 confocal images of retinal plexus in dorsal retina of WT (J) and cKO (K) stained with IB4 (green)
586 and anti-CD31 antibody (red). (L,M) Transverse cryostat sections of P26 retina stained with IB4
587 (green) and anti-GFAP antibody (red) to mark endothelial cells and astrocytes, respectively.
588 Superficial (S), intermediate (Int) and deep (d) vascular plexus are marked; outer nuclear layer
589 (ONL), inner nuclear layer (INL), and ganglion cell layer (GCL) can be seen with nuclei marker,
590 DAPI (blue). Note that the anti-GFAP (raised in mouse) antibody lightly stains vascular cells, as
591 these mice were not perfused.

592 **Figure 4. Fewer astrocyte precursors in *Tbx3* cKO retinas, starting as early as P2.**

593 (A,B) Endothelial cells are marked with IB4 (green) in WT and *Tbx3* cKO flat mounted retinas at
594 P2. (A',B') Same samples immunostained for astrocyte precursors using anti-PDGF receptor
595 alpha (PDGFRα) antibody. (C,D) Inverse images of flat mount retinas from P2 WT and *Tbx3*
596 cKO stained with a second astrocyte precursor marker, anti-Pax2 antibody (black). Red bar
597 marks Pax2-positive cells furthest away from the optic nerve head in each panel. Dashed yellow
598 box indicates images magnified in panels C',D'. (E) Quantitation of Pax2-positive cells furthest
599 away from optic nerve head in heterozygote (control, N = 4) and conditional knockout (cKO, N =
600 5) retinas. Distance was averaged measure of 10 cells per dorsal and another 10, ventral.
601 Statistical significance was determined using a 2way ANOVA with Tukey multiple comparisons
602 test; ****, $p < 0.0001$. (F) Graph showing quantitation of the percentage of surface area occupied
603 by dorsal and ventral retinas in control (grey) and cKO (white); statistical significance was
604 determined using a 2way ANOVA with Tukey multiple comparisons test; **, $p < 0.01$; N, number
605 of mice.

606 **Figure 5. Astrocyte lattice fails to form in dorsal-temporal *Tbx3* cKO retina.**

607 (A,B) Flat mount P9 retinas immunostained with mature astrocyte marker, anti-glial fibrillary
608 acidic protein (GFAP) antibody. Arrows point to the hyaloid artery (HA). (C,D) Flat mount P30
609 retinas from WT and cKO mice. (D) Arrows indicate lattice thinning. (D'-D''') Magnified view of
610 boxed region in (D) shows dorsal region where astrocyte lattice fails to reach the retinal edge.
611 (D') Astrocytes, GFAP (orange); (D'') endothelial cells, IB4 (green); and (D''') overlay. (E) Graph
612 quantifying the normalized ratio of astrocyte occupation compared to the retinal surface area for
613 WT and cKO retinas. Dorsal is up in all panels; statistical significance was determined using an
614 ordinary 2way ANOVA with Tukey multiple comparisons; ****, $p \leq 0.000.1$; ***, $p \leq 0.001$; N,
615 number of mice.

616 **Figure 6. Dorsal specific loss of RGCs with loss of *Tbx3*.**

617 (A) Snapshot of whole eyes with optic nerves from P9 WT and cKO siblings. (B,C) Sections of
618 WT and cKO eyes stained with nuclei marker (DAPI) to visualize neural retina. Dashed line
619 indicates optic nerve thickness in each sample. (D) Graph quantitating the optic nerve thickness
620 in WT and cKO eyes. Statistical significance was measured using an unpaired, two-tailed T-test;
621 **, p = 0.005. (E-F) Transverse cryostat sections of P9 WT and cKO dorsal tip immunostained
622 with anti-Islet1/2 antibody. The number of Islet1/2-positive cells in the first 300µm of the most
623 dorsal and ventral retina were counted (dashed line). (G) Graphs of the Islet1/2-positive cells in
624 the dorsal and ventral regions. (H-I') Inverse images of P9 flat mount WT and cKO retinas
625 immunostained with anti-OPN4 antibody marking intrinsically photosensitive ganglion cells
626 (ipRGCs). Dashed box shows area magnified in H' and I'. Density of cells were measured in
627 dorsal, nasal/temporal (N/T) and ventral petals and normalized to WT siblings. (J) Graphs
628 showing quantitation of OPN4-positive cells in each region. (K) Inverse image of P30 cKO flat
629 mount with magnified area (dashed box) shown in panel K'. (L) Graphs of OPN4-positive cells
630 per whole retina of P9 and P30 samples (WT, N = 4; cKO, N=3). An unpaired, two tailed T-test
631 were used to determine statistical significance; p-values on graphs in panels G,J,L; N, number
632 of mice.

633 **Supplemental Figures, Tables & Movies**

634 See attached file Supplemental Materials file

Figure 1

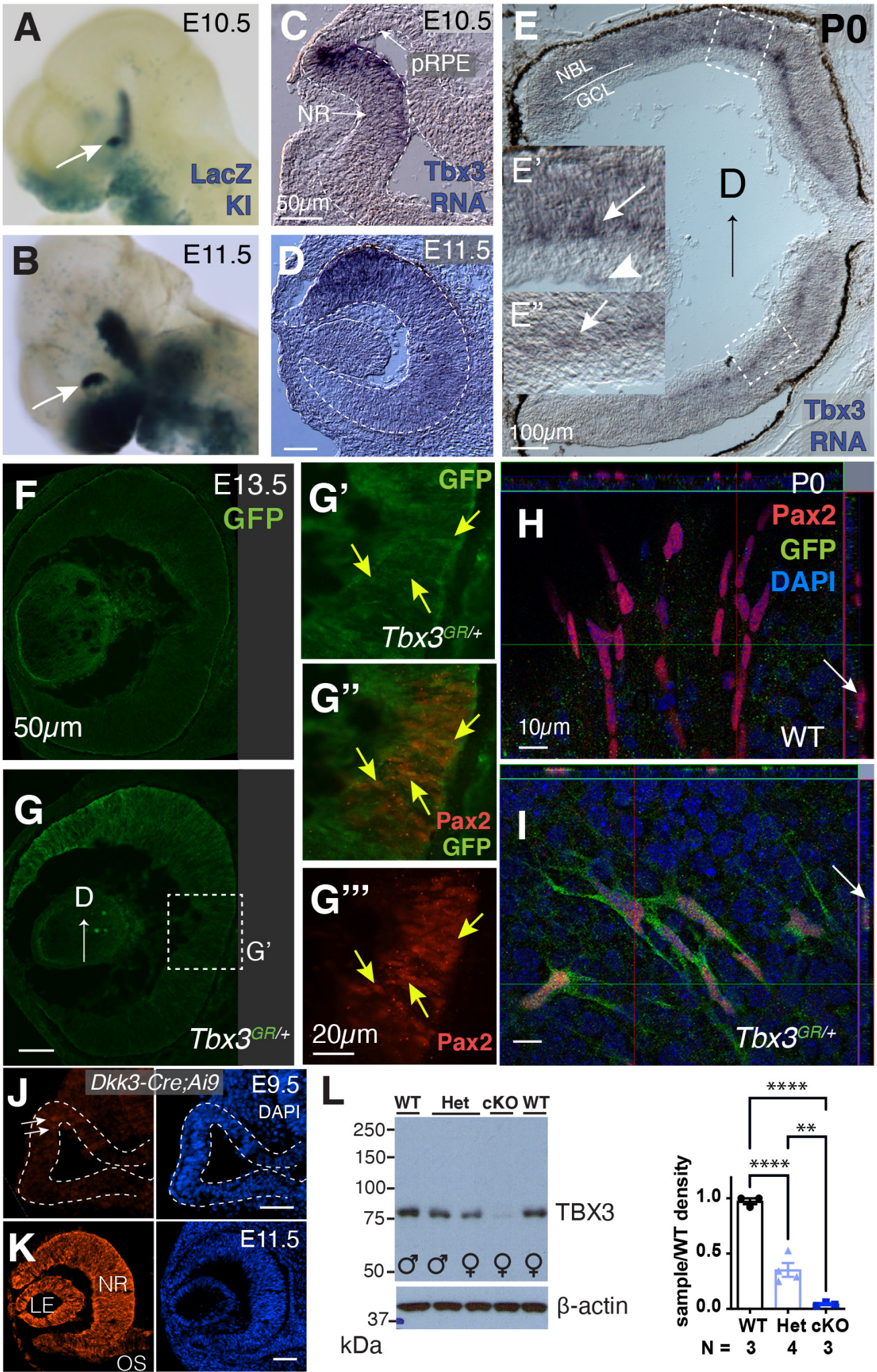
A
E10.5
LacZ
KI
B
E11.5
C
E10.5
pRPE
NR
Tbx3
RNA
50μm
D
E11.5
E
P0
NBL
GCL
E'
D
E''
Tbx3
RNA
100μm
F
E13.5
GFP
50μm
G'
GFP
Tbx3GR/+
G''
Pax2
GFP
G'''
Pax2
20μm
G
D
G'
Tbx3GR/+
H
P0
Pax2
GFP
DAPI
10μm
WT
I
Tbx3GR/+
J
Dkk3-Cre;Ai9
E9.5
DAPI
K
E11.5
NR
LE
OS
L
WT
Het
cKO
WT
250
150
100
75
50
37
kDa
TBX3
β-actin
sample/WT density
1.0
0.5
0.0
****
**
****
WT
Het
cKO
N = 3
4
3

Figure 2

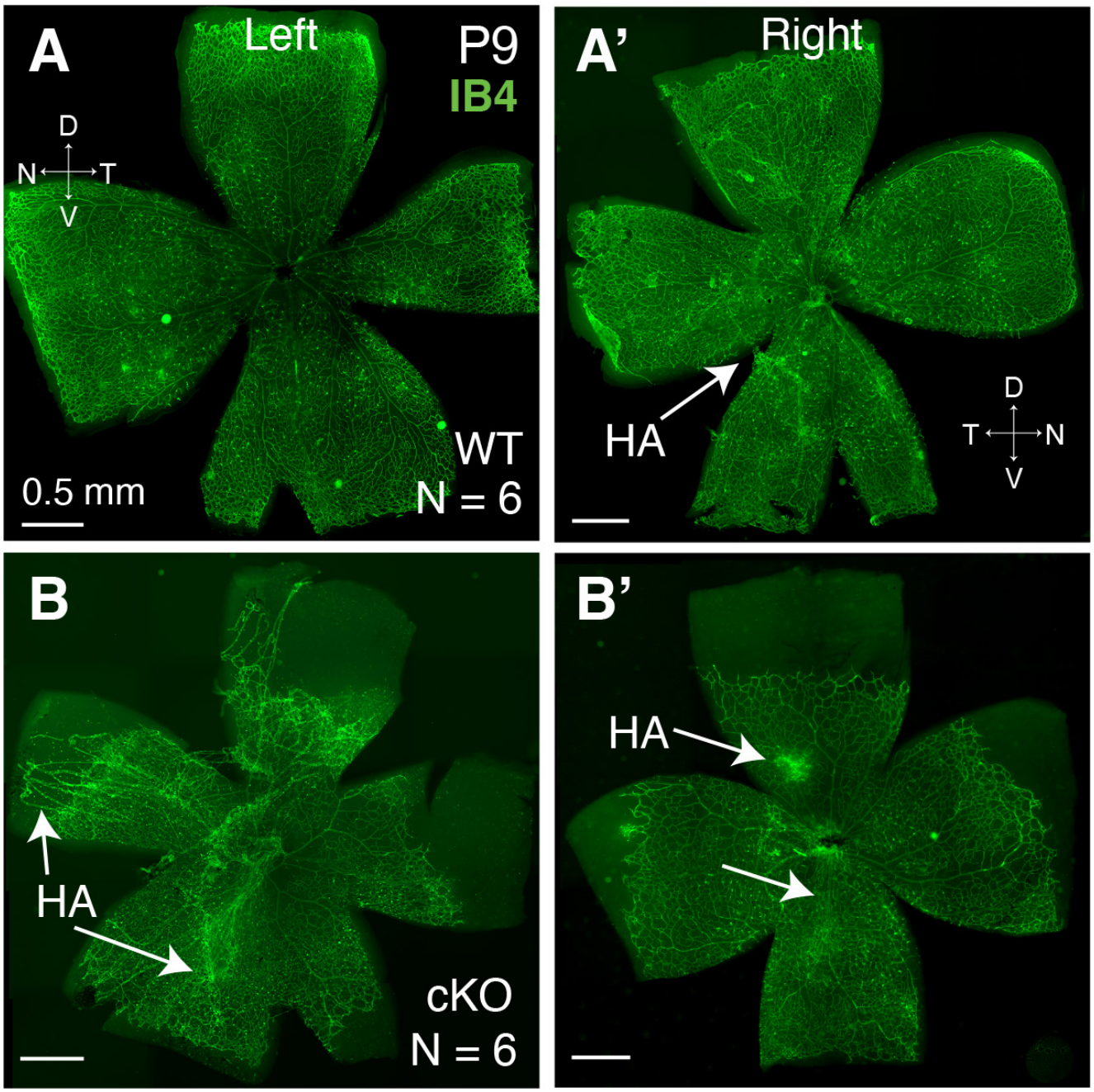
A
Left
P9
IB4
D
N
T
V
WT
N = 6
0.5 mm
A'
Right
HA
D
T
N
V
B
HA
cKO
N = 6
B'
HA

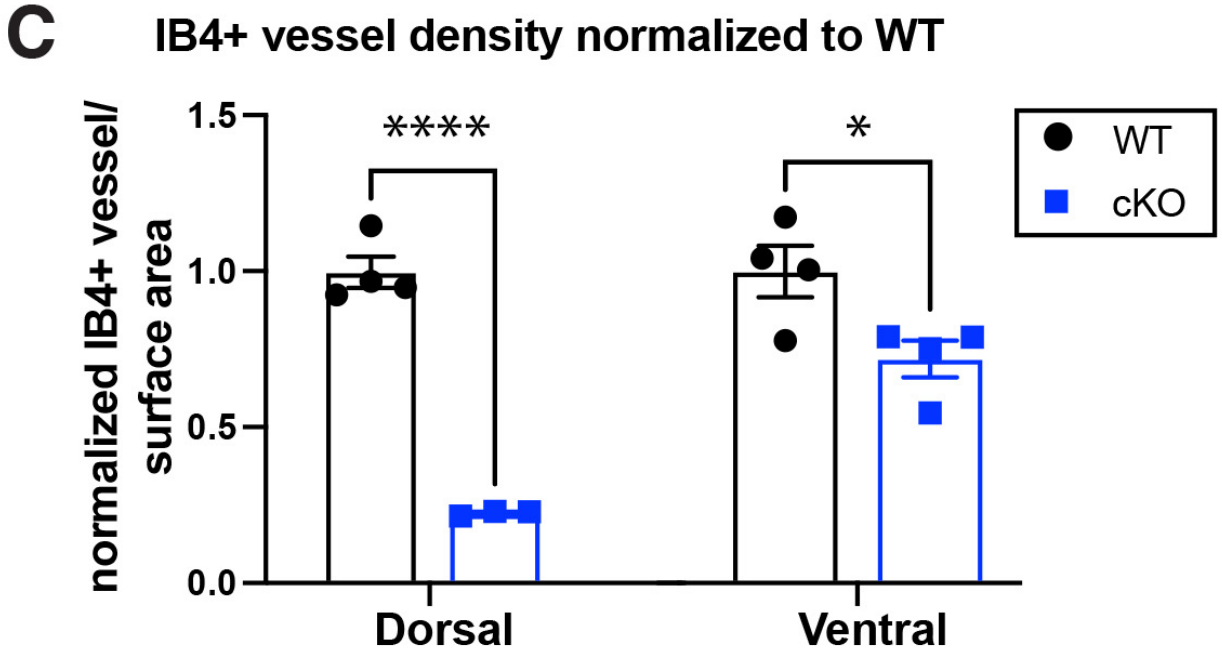
C
IB4+ vessel density normalized to WT
normalized IB4+ vessel/ surface area
1.5
1.0
0.5
0.0
****
*
WT
cKO
Dorsal
Ventral

Figure 3

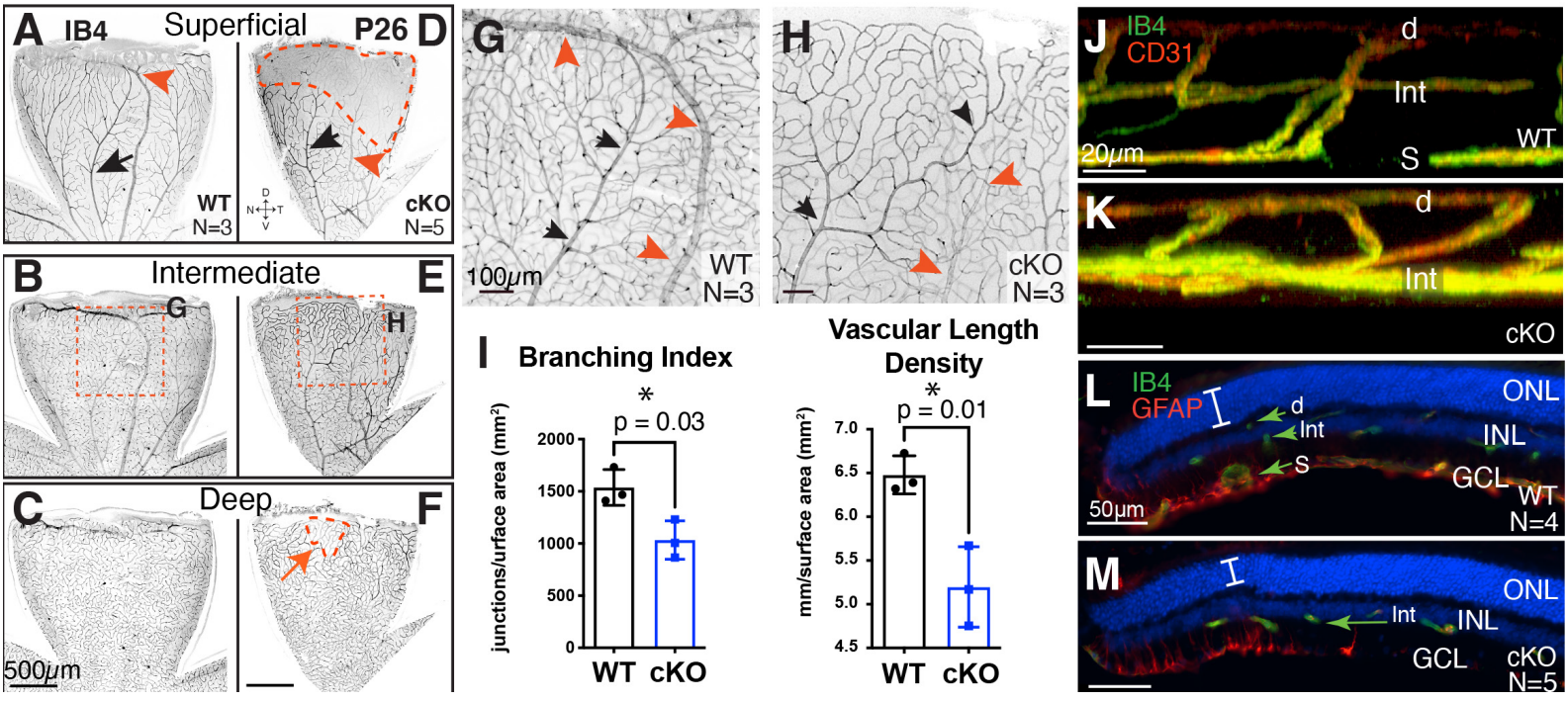

Figure 4

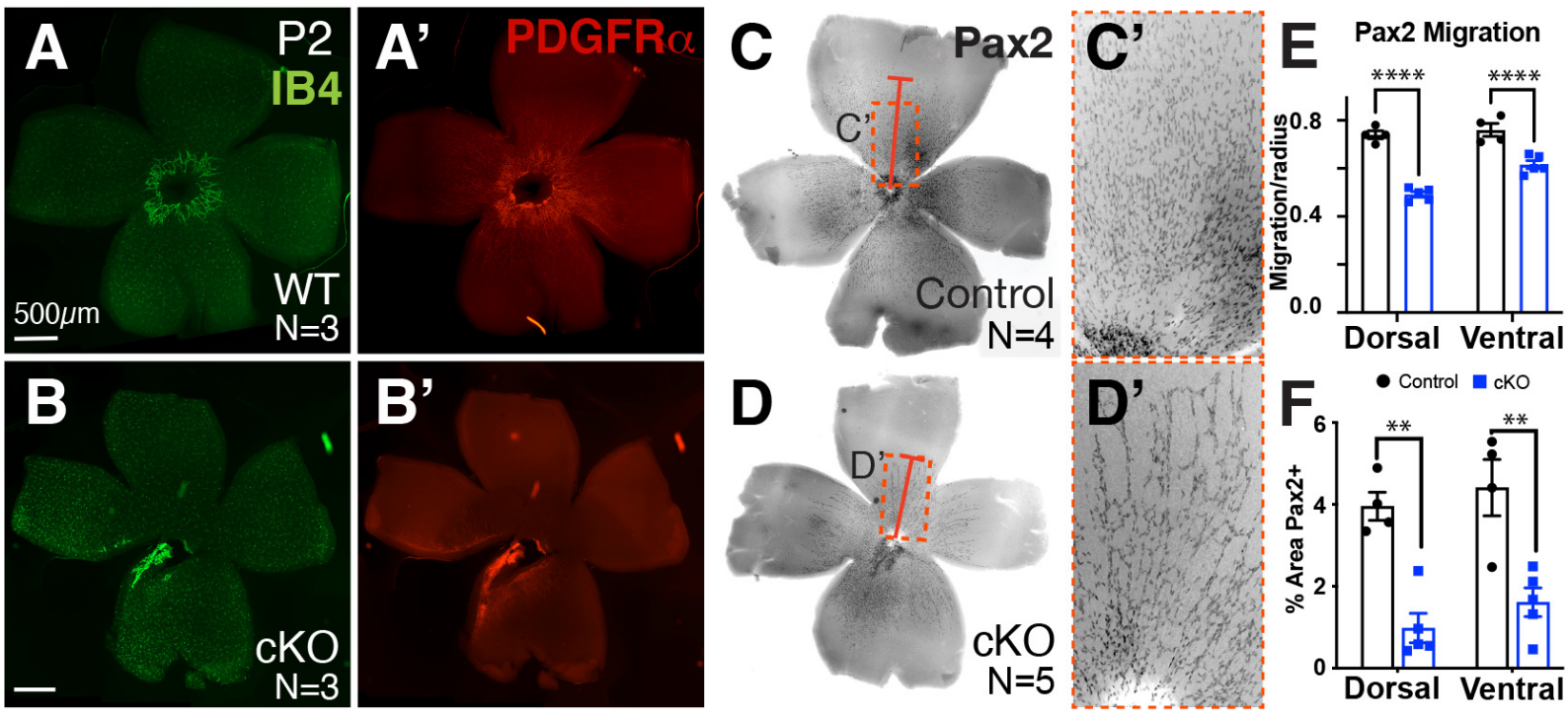

Figure 5

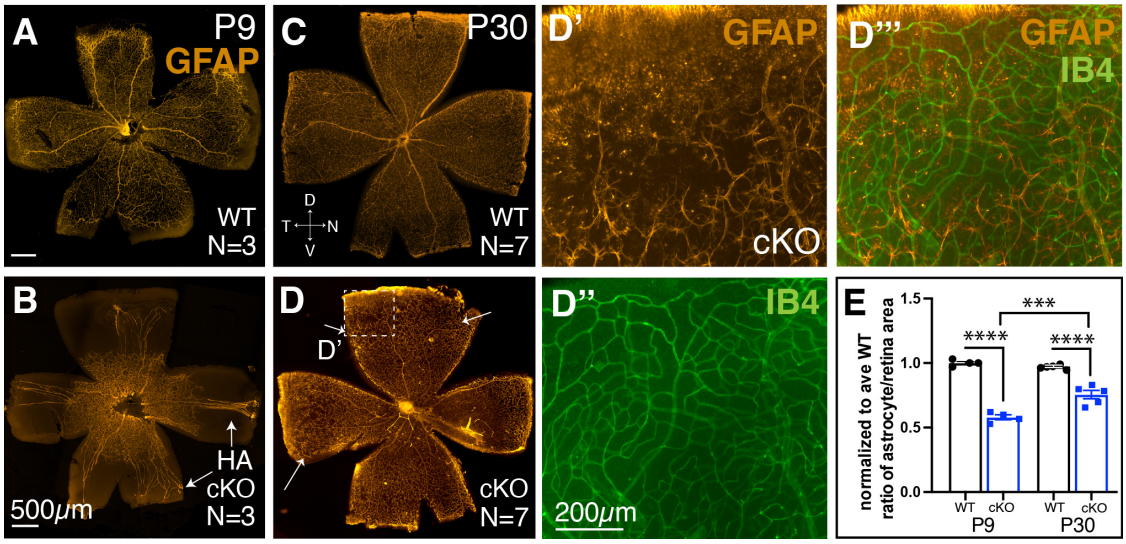
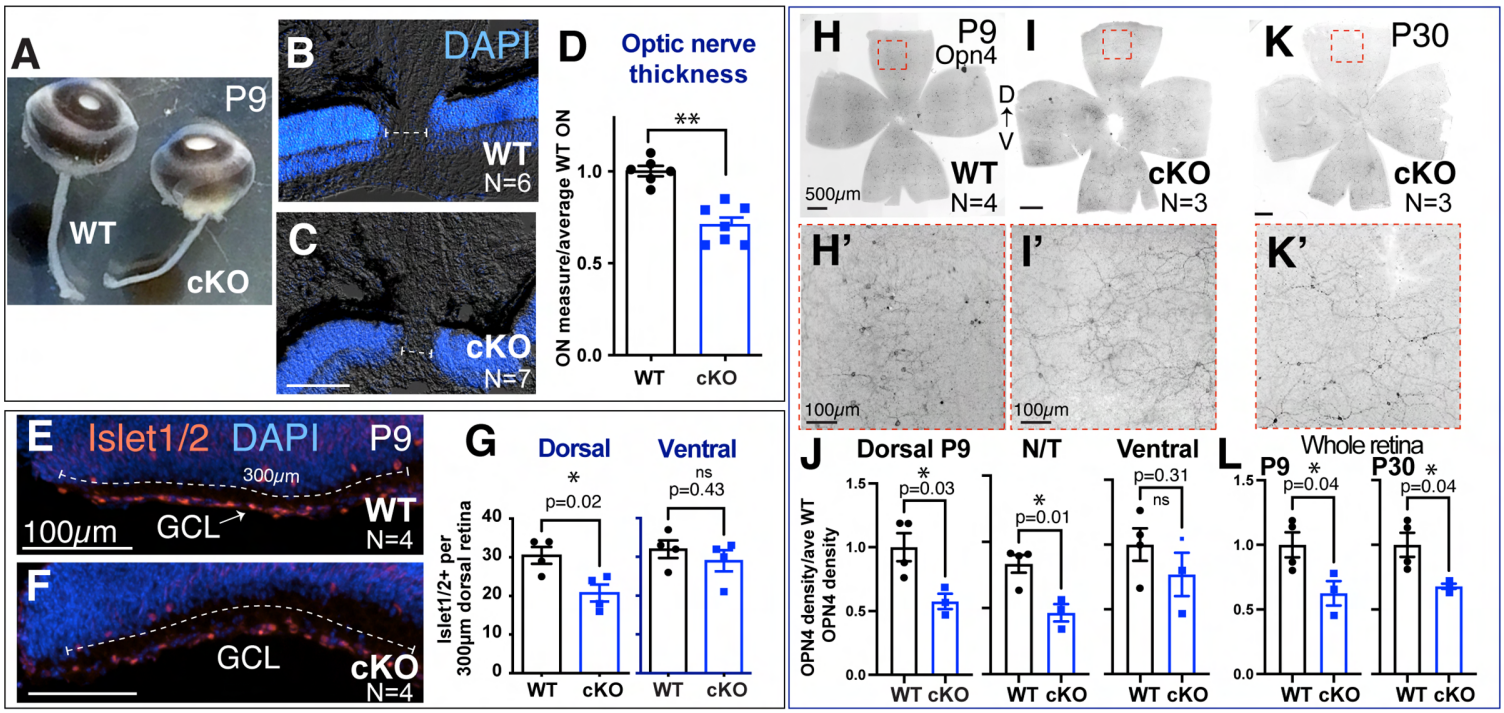
Figure 6